

Research paper

Enhanced mechanical properties of the high-resolution EUVL patterns of hybrid photoresists containing hexafluoroantimonate

Pawan Kumar^a, Pulikanti Guruprasad Reddy^b, Satinder K. Sharma^{a,*}, Subrata Ghosh^b, Chullikkattil P. Pradeep^b, Kenneth E. Gonsalves^{b,*}

^a School of Computing and Electrical Engineering, Indian Institute of Technology (IIT)-Mandi, H.P. 175005, India

^b School of Basic Science, Indian Institute of Technology (IIT)-Mandi, H.P. 175005, India

ARTICLE INFO

Keywords:

Extreme ultraviolet (EUV) lithography
Novel nonchemically negative tone (n-CARs) resists
Low activation energy
Optimum dose
Sub 20 nm technology node
Next generation lithography
Adhesion
Modulus
Patterns collapse

ABSTRACT

The present study investigates the mechanical properties of hybrid photoresists in the context of their pattern-collapse behaviors. The mechanical properties such as the DMT (Derjaguin, Muller, Toropov) modulus and tip-sample adhesion forces of the high-resolution patterns obtained from two hybrid EUV photo-resists, 1.5% & 2.15%-MAPDSA-MAPDST bearing hexafluoroantimonate and triflate counter ion moieties have been investigated using peak force quantitative nano-mechanical mapping (PF-QNM) technique. The mechanical properties of the well resolved high-resolution 90–20 nm (L/5S) line patterns, 20–32 nm (L/2S-L/5S) lines patterns and nano-features such as line-elbow connections have been investigated and analyzed against the differences in their SbF_6^- composition. For the 1.5%-MAPDSA-MAPDST resist case the DMT modulus and tip-sample adhesion forces are found strong dependence on the resist line width and line spacing, as compared to 2.15%-MAPDSA-MAPDST resist. There is a significant improvement in the modulus value of 5 GPa for 2.15%-MAPDSA-MAPDST resist in contrary to the ~ 2.7 GPa for the 1.5%-MAPDSA-MAPDST resist for the 20 nm (L/2S) Line patterns. Similarly, the tip sample adhesion forces on resist surface are also found dependent on patterns aspect ratio as well as on SbF_6^- content in the resist composition. These studies revealed that an increase of the SbF_6^- content in the resist formulation, imparts cascading effects to the mechanical properties of their high-resolution nanopatterns, which in turns helps to reduce the pattern collapse resulting in superior patterning performances.

1. Introduction

The semiconductor industries over the years have made remarkable progress in the miniaturization and performance enhancement of devices with the advancement of integrated circuit (IC) technology, which helped in reducing the device size promoting higher device density, clock rate, and also transistor switching rate [1–5]. However, the growth of IC technology faces constraints when the feature dimensions reach nanometer regime due to the inherent limitations of various nanofabrication technologies available [5,6]. High-resolution lithographic techniques currently employed for the nano-scale fabrication of devices include deep ultraviolet (DUV), electron beam (e-beam), He ion beam, 193 nm immersion, X-ray and extreme ultraviolet lithography (EUVL) [7–11]. Among these, EUVL, which uses 13.5 nm wavelength for patterning, is a major contender for the next generation sub-10 nm technology node lithography [10,11]. However, the successful implementation of EUVL for nano-scale patterning requires high-end

photoresists capable of patterning high-resolution features at high aspect ratios [4,12]. Therefore, semiconductor industry and scientific community have focused their attention on the development of novel EUVL resist materials in recent years [4,10,13–20]. However, the design and development of a high-end photoresist is a formidable task due to a variety of problems observed in high-resolution patterning such as line fracturing, buckling, folding, peel-off and pattern-collapse [21–23]. Especially, the pattern collapse observed for high aspect ratio line patterns (sub-20 nm) is a major challenge in next-generation EUVL applications [21]. Therefore, understanding the factors behind the pattern-collapse behaviors exhibited by resists at higher resolutions is critical in evaluating the resolution limit, particularly for sub-20 nm technology nodes [21,23]. Factors such as capillary forces acting on high-resolution resist patterns during the rinsing or development processes are known to cause pattern collapse [24]. Other factors that may influence the pattern collapse include the feature size, resist thickness, resist modulus, resist adhesion to the substrate and swelling behavior of

* Corresponding authors.

E-mail addresses: satinder@iitmandi.ac.in (S.K. Sharma), kenneth@iitmandi.ac.in (K.E. Gonsalves).

the resist [24]. The minor changes in the developer contact angle significantly affect the capillary forces on the resist side walls and leads to the feature collapsing behaviour at higher resolution nodes [25–28]. Therefore, two main requirements to prevent the pattern collapsing behaviour of the resist is: 1) reducing the surface tension of the developer 2) increasing the resist hardness. However, the contact angle of high resolution resist patterns is very difficult to measure and depends on the forces of adhesion on the surface in contact. Hence the measuring the surface adhesion forces of the patterned resist features is an indirect measure of the contact angle [29]. Therefore, the resist with high modulus and high surface adhesion forces can reduce the capillary forces considerably during drying process [24].

Structural engineering is one of the methods to improve the modulus and adhesion properties of the resist. The incorporation of crosslinkers in photoresist materials is known to improve their mechanical strength, resulting in collapse free patterns [24,25,30]. However, the addition of crosslinkers may result in adverse effects like line swelling [24,31–33]. Therefore, alternative methods such as the development of organic-inorganic hybrid resists have been explored toward the development of collapse free patterns at higher resolution nodes [4,15–18]. It has already been shown that the incorporation of inorganic components in the resist formulation helps to improve sensitivity and resolution [23]. In addition, the inorganic components in photoresist formulations are known to increase their optical density by harvesting EUV photons more efficiently leading to superior lithographic performances [4,23]. Therefore, the development of new hybrid n-CARs for high-resolution EUV lithographic applications and investigation of their mechanical properties is extremely important for future semiconductor industries.

However, the mechanical properties such as the modulus and adhesion are relatively hard to evaluate at nano-scale regime where the bulk properties disappear and various interface contributions start to dominate [34]. There are only a few reports on the evaluation of modulus of a photoresist material with respect to its pattern collapse behaviors [23,24,35]. Winroth et al. extracted the intrinsic stress of the exposed resist patterns by calculating the lateral force required to break the resist lines by using AFM technique [34]. However, these methods are tedious, time-consuming and also result in the destruction of the resist patterns. The Peak Force Quantitative Nano-mechanical Mapping (PF-QNM) method is a non-destructive technique capable of quantifying DMT (Derjaguin, Muller, Toropov) modulus and tip-sample adhesion forces with high spatial resolution [36,37].

Considering the above facts, the present study demonstrates the effect of varying concentrations of an inorganic moiety, hexafluoroantimonate (SbF_6^-), in hybrid resist formulations on the mechanical properties such as modulus and adhesion of their patterns. To accomplish this, we have developed two different hybrid copolymer resists 1.5% & 2.15%-MAPDSA-MAPDST (where MAPDSA = (4-(methacryloyloxy)phenyl)dimethylsulfonium hexafluoroantimonate and MAPDST = (4-(methacryloyloxy)phenyl)dimethylsulfonium triflate) containing different percentages of SbF_6^- counter ion moiety for higher resolution EUVL applications (1.5% and 2.15% resists hereafter). We included MAPDST in the hybrid resist because it is known to undergo polarity change on EUV exposure by the conversion of hydrophilic sulfonium triflates into hydrophobic sulfide functionality during the lithography process. Our earlier studies have also shown that the introduction of SbF_6^- moiety in the formulation helps to improve the sensitivity of the photo-resist [38]. Consequently; the obtained nano-features were subjected to mechanical studies by using non-destructive PF-QNM technique. Furthermore, the effect of the aspect ratio on mechanical properties of high-resolution line patterns has also been studied by a quantitative mapping of the variations in modulus and tip-sample adhesion force values.

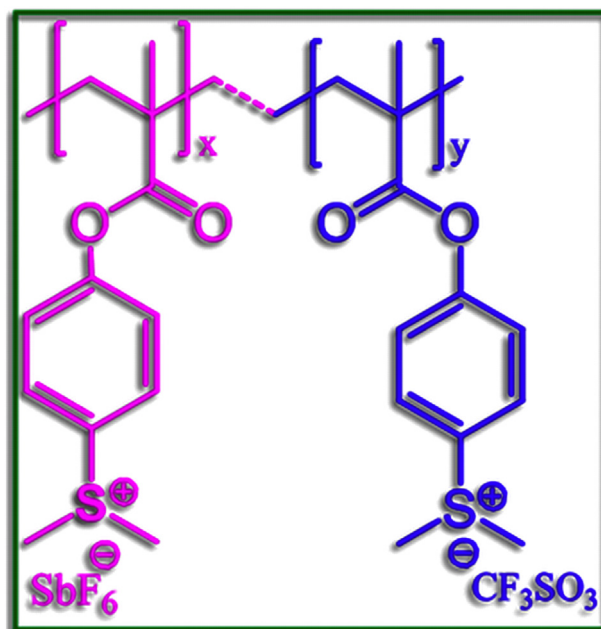


Fig. 1. Chemical structures of the MAPDSA-MAPDST copolymer resist.

2. Material and methods

2.1. Materials

The hybrid copolymer resists 1.5% & 2.15%- MAPDSA-MAPDST (1.5% and 2.15% resists) with a chemical structure shown in Fig. 1 were synthesized and characterized according to our published procedure [38,39]. The FT-IR profiles for 1.5% and 2.15% resists were given in the Supplementary material (see, Figs. S1 and S2).

2.2. Thin film preparation, and EUV exposure

Resist solutions were prepared by dissolving solid 1.5% and 2.15% resists (3 wt%) in acetonitrile followed by filtration through 0.2 μm Teflon filters. Smooth resist thin films of ~ 45 nm thickness were achieved by spin coating the resist solutions onto 4", p-type silicon substrates at 4500 rpm for 60 Sec. Thereafter, thin films were subjected to pre-exposure bake at 60 °C for 60 s. EUV exposures on the resist films were performed by using a micro-exposure tool (MET) at the Advanced Light Source (ALS) in Lawrence Berkeley National Laboratory (LBNL) using ALS MET Standard low flare bright-field R4C3 Mask IMO228775. A post exposure bake was applied on the EUV exposed resist films at 65 °C for 60 s. Thereafter, resist films were developed with 0.02 N tetramethylammonium hydroxide (TMAH) solution for 15 s, followed by DI water rinsing for 10 s. Due to the over development of resist nano-features in industrial standard 0.26 N TMAH, we used dilute 0.02 N TMAH as the developer in the present study. The calculated center dose and sizing dose values for 1.5% and 2.15% resists were 41 & 96 mJ/cm² and 11 & 33 mJ/cm², respectively [34].

2.3. FE-SEM and AFM characterization details

Field Emission Scanning Electron Microscope (FE-SEM Carl Zeiss, Ultra Plus) and Atomic Force Microscopy (AFM-Dimension Icon, Bruker) were utilized for investigating the critical dimensions (CD) of the line and other nano-patterns obtained from the 1.5% and 2.15% resists.

2.4. Line edge roughness and sensitivity calculations

The line edge roughness (LER) of the EUV patterns obtained from 1.5% and 2.15% resists was calculated by using SUMMIT® software. The obtained LER values measured on SEM images for 20 nm (L/5S) line patterns of these resist formulations were 1.53 ± 0.22 nm and 5.18 ± 1.57 nm, respectively. The sensitivity and contrast values for 1.5% and 2.15% resists were calculated as 58.1 mJ/cm^2 & 0.036 and 24.5 mJ/cm^2 & 0.07, respectively, from the normalized remaining thickness (NRT) curve analyses (see, Supplementary material, Fig. S3(a)–(b)) [38]. In both the cases, a gradual increase in the residual film thickness was observed with increase in the exposure dose values, confirming the negative tone nature of the resists.

2.5. Mechanical property analysis

In order to understand the mechanism behind the high-resolution pattern collapse, the mechanical analysis of the developed resist patterns were performed by using AFM technique operating in peak force tapping mode. The standard AFM cantilever (TESPA) from Bruker having ~ 8 nm nominal tip radius, ~ 325 kHz resonant frequency and 42 N/m spring constant with a tip half angle of 18° was used for PF-QNM measurements of the resist patterns. By deflection sensitivity calibration, the cantilever spring constant and the tip radius were estimated. A force-distance curve as shown in Fig. 2 was calculated, which gives quantitative information about the elastic modulus, tip-sample adhesion forces etc. The standard relative method was used for the measurement of mechanical properties using polystyrene (PS) thin film ($\sim 1 \mu\text{m}$) as a reference of known Young's modulus value, $\sim 2.8 \text{ GPa}$ [40]. The PF-QNM measurements were performed on reference sample followed by peak force set point adjustments in order to get the desired deformation (2–5 nm). After this procedure, the tip radius parameter was adjusted such that the modulus of the PS reference sample corresponded to its standard value. Having measured the reference samples as above, the PF-QNM measurements on the MAPDSA-MAPDST resist patterns were carried out by adjusting the peak force set-point such that the deformation matched with the reference sample (2–5 nm). Herein, the AFM images (of 512×512 pixels) were captured at a scan rate of 0.6 Hz and analyzed & processed by using Nanoscope Analysis (Ver. 9) software. In order to eliminate the unwanted features such as noise, bow and tilt from the scan line, the AFM topography images were processed by using the flatten tool with Nanoscope Analysis software. On the other hand, no reduction process is applied to the modulus as

well as adhesion mapping images as those are quantitative properties and measured by using the standard relative method. In PF-QNM technique, z-piezo sensor taps on the surface of the sample and measures the force-distance curve at every tap. From the force-distance curve, one can determine modulus, the maximum adhesion force between the AFM tip and the resist sample surface as well as the amount of energy that was dissipated during the measurement as depicted in Fig. 2. Additionally, the elastic modulus of MAPDSA-MAPDST resist formulations can be obtained by fitting the DMT model to the section of the force-distance curve where the resist sample and the tip are in contact and by measuring the adhesion forces between the tip and resist sample using the following equation [36,37]:

$$F_{\text{Tip}} = \frac{4}{3} E_r \sqrt{Rd^3} + F_{\text{adh}} = k(x) \quad (1)$$

where, E_r , F_{adh} , d , R , k and x are the reduced modulus, adhesion forces between the tip and the resist sample, deformation on the resist sample surface at peak force, tip radius, cantilever spring constant and vertical displacement of the cantilever, respectively. Thus, from Eq. (1), the reduced modulus (E_r) is computed by the following relation [37]:

$$E_r = \frac{3(F_{\text{Tip}} - F_{\text{adh}})}{4\sqrt{Rd^3}} \quad (2)$$

The reduced modulus (E_r) is related to Young's modulus (E_s) of the resist sample as:

$$\frac{1}{E_r} = \frac{1 - \nu_s^2}{E_s} + \frac{1 - \nu_{\text{Tip}}^2}{E_{\text{Tip}}} \quad (3)$$

where E_{Tip} and ν_{Tip} are Young's modulus and Poisson's ratio of the AFM tip and ν_s is the Poisson's ratio of the resist sample. The contribution of the second term in Eq. (3) is negligible since, $E_{\text{Tip}} \gg E_s$.

3. Results and discussion

Fig. 3(a) & (b) shows the AFM topography of 20 nm line features obtained from 1.5% and 2.15% resists at various critical dimensions (CD) starting from L/2S to L/5S (line/space), respectively. From these figures, it can be seen that the L/5S, L/4S, and L/3S line patterns are well resolved in the case of 1.5% resist, but the line patterns collapse as the L/S value approaches L/2S. Whereas, in the case of 2.15% resist, the high-resolution line patterns (L/5S, L/4S and L/3S) are well resolved and the pattern collapse is not observed even for L/2S (Fig. 3(b)) line patterns. Similar behaviour is also observed in the case of 22 nm line patterns obtained from 1.5% and 2.15% resists for L/5S–L/3S features (see, Supplementary material Fig. S4(a)–(b)).

Nano-features such as dots, boats, waves, star-elbows, rings etc., are of special interest in lithography, as such features find applications in a wide range of areas including high-density magnetic recording, photonic crystals, information storage, micro-lens arrays, tissue engineering and catalysis [41]. The Fig. 3(c) and (d) shows line-elbow connections nano-patterns obtained from 1.5% and 2.15% resists respectively under EUVL conditions. As seen from Fig. 3(c) and (d) the 40 nm line-elbow connections of the 1.5% resist was showing buckling than that of the 2.15% resist patterns. While analyzing these results, it appears that the 2.15% resist exhibits better performance as compared to 1.5% resist under the given set of experimental conditions.

It was reported that pattern collapse exhibited by the higher resolution resist patterns depends on the modulus as well as on the surface properties (hydrophilic nature) of the resist patterns [26–28]. As discussed above, pattern collapse occurs during the resist development and rinsing process due to existing capillary forces on side walls of the resist patterns. The critical aspect ratio for the patterns collapse is linearly dependent on the spacing between the resist line and the pressure difference across a capillary meniscus can be given by the Laplace equation [26];

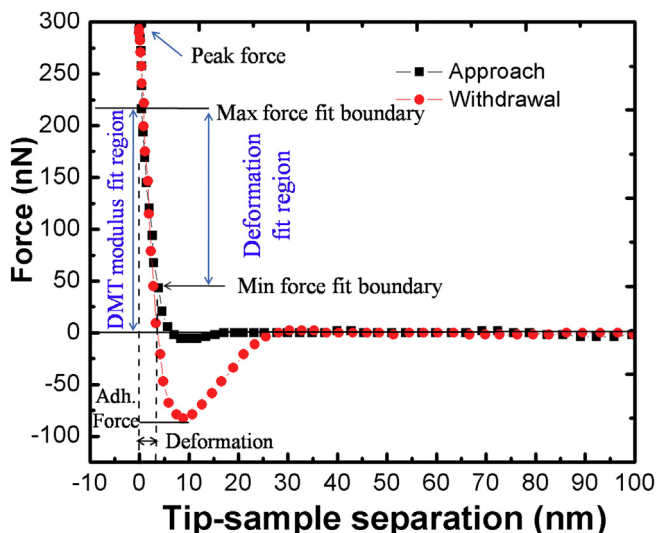


Fig. 2. The force-distance curve for the approach and withdrawal of the AFM tip during the PF-QNM measurement.

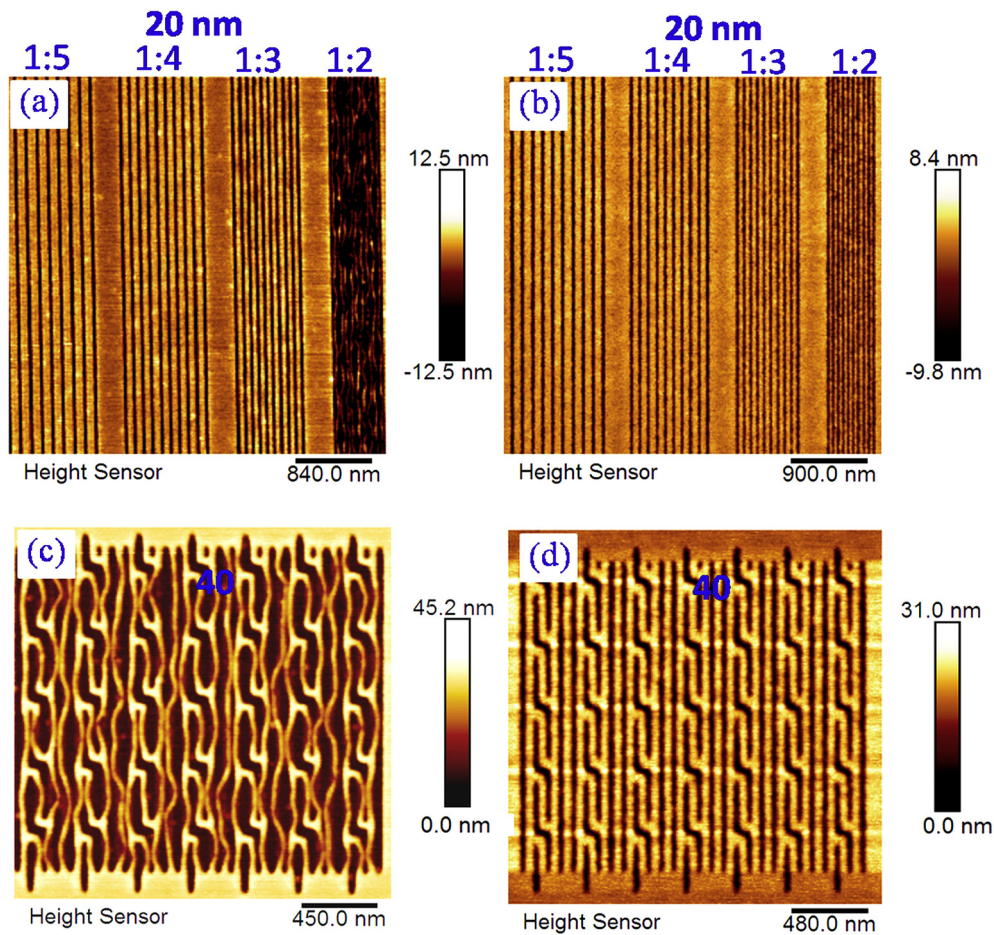


Fig. 3. AFM topography of the 20 nm line patterns for (a) 1.5% resist; (b) 2.15% resist with different (line/space) features starting from L/2S to L/5S, and high resolution AFM topography images of 40 nm line-elbow connections for (c) 1.5% resist; (d) 2.15% resist patterns.

$$\Delta P = \frac{\gamma}{R} \tag{4}$$

where ΔP , γ and R are the Laplace pressure gradient, surface tension and radius of curvature respectively. Also the radius of curvature of meniscus depends on the distance between two photoresist line (S) as [26],

$$R = \frac{S}{2 \cos \theta} \tag{5}$$

where, S is the spacing between the feature and θ is the contact angle [26].

From the Eqs. (4)–(5), it is clear that a small change in the contact angle has large effect on the value of the critical aspect ratio for the patterns collapse, if the contact angle of the water approach 90° , the magnitude of the capillary forces will decay to zero [26–28]. Therefore, the resist with the hydrophilic surface (with high surface adhesion forces) might have ability to reduce the capillary forces which in turn reduce the patterns collapse as well. Therefore, in order to get collapse free patterns, the resist should possess the high stiffness (high modulus) and low capillary forces (hydrophilic or high surface adhesion) during the rinse and drying process.

Considering the above, in the present study we have systematically investigated mechanical properties of the patterns obtained from 1.5% and 2.15% resist formulations by measuring their modulus and tip-sample adhesion forces using PF-QNM technique with DMT model to comprehend the pattern collapse properties exhibited by these resists.

Topography, DMT modulus and tip-sample adhesion of the 45, 40, 35, 30, 25, and 20 nm line features (L/5S) obtained from 1.5% resist and their corresponding line profile measurements were shown in

Fig. 4(a)–(c). These analyses reveal a gradual decrement in the DMT modulus values was noticed from 5 GPa to 3 GPa for the line patterns from 45 nm to 20 nm respectively. This significant reduction in the modulus of the high-resolution line features was also confirmed from the line profile measurement data as shown in Fig. 4(b). Tip-sample adhesion forces value of the patterned resist feature from 45 nm to 20 nm also following the similar trend as 40 nN to 35 nN respectively, see Fig. 4(c). Similar decay in the apparent Young modulus with resist patterns size was observed previously by Böhme et al. (2002) [27], for the resist patterns formed by chain scission & chain dissolution method.

Similarly, the mechanical property analyses were also conducted for 2.15% resist as well, see Fig. 4(d)–(f). It is clear from the DMT modulus image of Fig. 4(e) that there is no significant variation in the DMT modulus values of the patterned line patterns from 40 to 20 nm (L/5S) feature sizes. A similar trend was also observed in the case of tip-sample adhesion force of the resist line patterns (see Fig. 4(f)). These studies indicate that the 2.15% resist patterns show considerable improvement in both the modulus and tip-sample adhesion force values as compared to 1.5% resist patterns. The results obtained from 2.15% resists were also compared with few existing literature reports, for example, Delcambre et al. (2010) [28] studied the effect of the 5% antiplastisizing agent (Tris(2-chloropropyl phosphate) in PMMA nanostructure reveal that improved modulus value from 3.9 GPa (in the pure sample) to 4.9 GPa. In addition, Torres et al. (2010) also studied that due to addition of 5% dioctyl phthalate (DOP) in PS and PPMA leads to the increase in the modulus at the nanoscale [42]. Therefore, incorporated inorganic counter ion (SbF_6^-) acts as an antiplastisizer in the hybrid resist formulations and helped to increase the mechanical properties of the patterned resist features. The calculated modulus value for the bulk

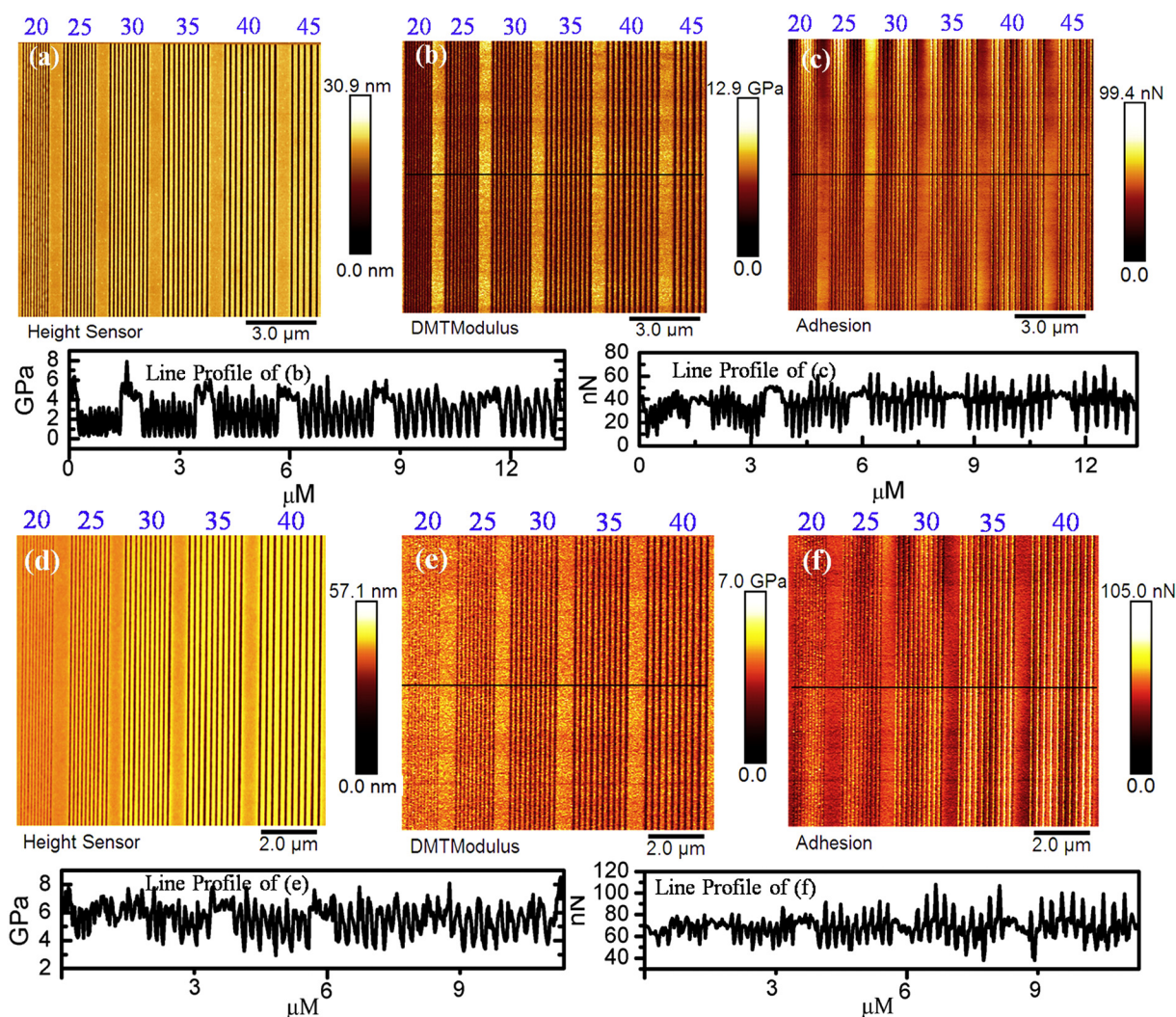


Fig. 4. (a) Topography; (b) DMT modulus; (c) tip-sample adhesion, mapping images of the 1.5% resist lines of 45, 40, 35, 30, 25 and 20 nm feature sizes (L/5S) with corresponding line profile measurements; (d) topography; (e) DMT modulus; (f) tip-sample adhesion, mapping images of the 2.15% resist lines of 40, 35, 30, 25 and 20 nm feature sizes (L/5S) with corresponding line profile measurements.

in between the grating of 1.5% and 2.15% MAPDSA-MAPDST resist were 5 GPa and 6.5 GPa respectively. In addition, the corresponding adhesion forces values were 45 nN and 60 nN respectively (see, Fig. 4).

The DMT modulus and tip-sample adhesion properties of the patterned hybrid resists (1.5% and 2.15% MAPDSA-MAPDST) were also measured at a lower scan area and reveals that no change in the mechanical properties of the resist features with scanning area. Comparison plots showing the variations in modulus and tip-sample adhesion force values measured on each lines patterns ranging from 20 to 90 nm features (L/5S) for 1.5% and 2.15% resists are given in Fig. 5(a) and (b), respectively.

Similarly, the Fig. 6(a) and (b) show the DMT modulus and tip-sample adhesion force plots for the 20 nm line patterns exhibited by 1.5% and 2.15% resists with different L/S characteristics ranging from L/5S to L/2S respectively. Although, an overall pattern collapse was noticed in the case of 1.5% resist for its 20 nm L/2S (line/space) patterns, it was still possible to observe some partially collapsed line patterns clearly from the AFM image (see, Fig. 3(a)). Accordingly, we had measured the modulus and comparison plots showing the variations in modulus and tip-sample adhesion force values from the different positions of the partially collapsed line patterns of 1.5% resist. A considerable decrement in the modulus and tip-sample adhesion force parameters is observed in the case of 1.5% resist line features as compared to those of the 2.15% resist.

The comparison of the DMT modulus and tip-sample adhesion force measured for the 20–32 nm (L/2S) lines patterns of 1.5% and 2.5% resists were shown in the Fig. 7(a) and (b) respectively. Fig. 7(a) shows the modulus decreases with the decreasing in the feature dimension of the 1.5% resist. On the other hand, the modulus values for 2.15% resist formulation remains constant at ~5 GPa. While, the tip-sample adhesion forces of 2.15% resist decreasing gradually with decrease in the critical dimension of the resist. Furthermore, the detailed DMT modulus and tip-sample adhesion exhibited by the of 1.5% and 2.15% resists at 20, 22, 28 and 32 nm line patterns (L/2S–L/5S) were given in Table 1. Interestingly, even at lower feature sizes such as 20, 22, 28 and 32 nm, the modulus and tip-sample adhesion force values of the 2.15% resist are higher than that of the 1.5% resist. All these results confirm a better performance of the 2.15% resist in terms of the mechanical properties of its high-resolution patterns as compared to those of the 1.5% resist patterns.

We have also performed mechanical measurements on nano-features obtained from 1.5% and 2.15% resists and the results obtained were given in Fig. 8 and Table S1 respectively. Fig. 8(a) shows the AFM topography image of the line-elbow connections of 1.5% resist, which indicate pattern collapse at higher resolutions. The corresponding DMT modulus and tip-sample adhesion force measured on the resist (arrows) were given in Fig. 8(b) and (c), respectively. The bright contrast observed in Fig. 8(b) and (c) are due to the silicon substrate or low

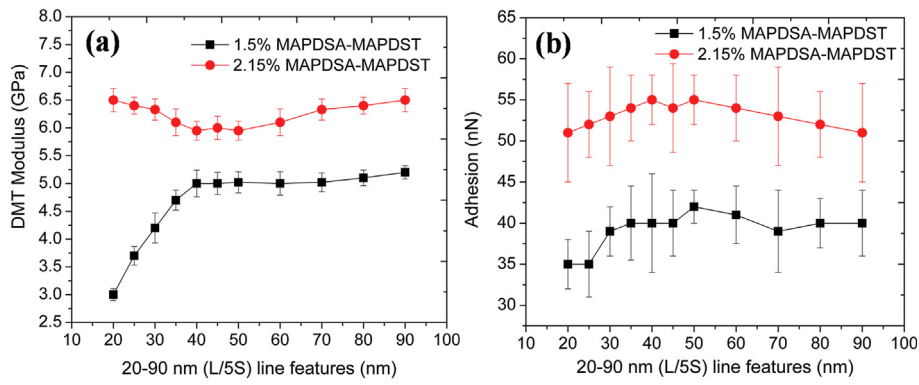


Fig. 5. (a) DMT modulus; (b) tip-sample adhesion force, plots for the 90–20 nm (L/5S) line features of 1.5% and 2.15% resists respectively.

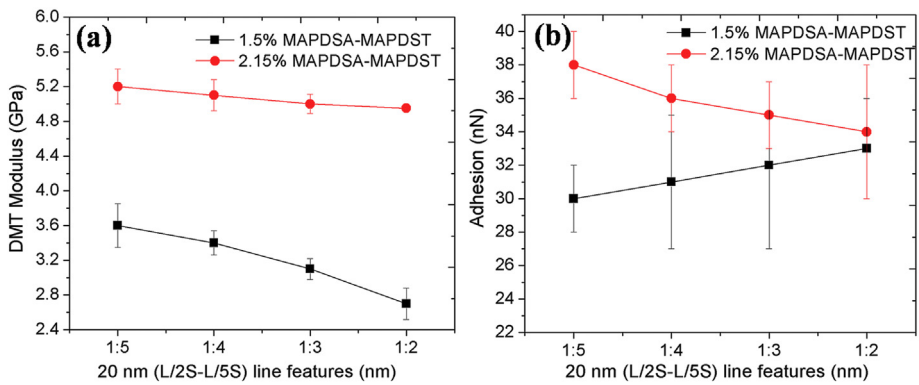


Fig. 6. (a) DMT modulus; (b) tip-sample adhesion force plots for the 20 nm line features (L/2S to L/5S) of 1.5% and 2.15% resists respectively.

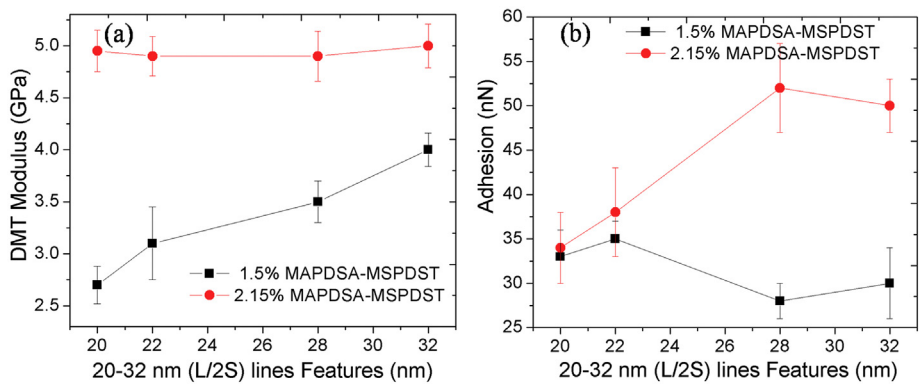


Fig. 7. (a) DMT modulus; (b) tip-sample adhesion force plots for the (20–32 nm) line features (L/2S) of 1.5% and 2.15% resists respectively.

Table 1

The DMT modulus (GPa) and tip-sample adhesion force (nN) values for 20, 22, 28 and 32 nm line features of 1.5% and 2.15% resists with different line/space characteristics in the range L/2S-L/5S.

Feature size	SbF ₆	(L/5S)		(L/4S)		(L/3S)		(L/2S)	
		DMT modulus	Adhesion						
20 nm	1.5%	3.6 ± 0.25	30 ± 3	3.4 ± 0.14	31 ± 4	3.1 ± 0.12	32 ± 5	2.7 ± 0.18	33 ± 3
	2.15%	5.2 ± 0.12	38 ± 2	5.1 ± 0.18	36 ± 2	5.0 ± 0.11	35 ± 2	4.95 ± 0.2	34 ± 4
22 nm	1.5%	3.9 ± 0.30	30 ± 5	3.75 ± 0.25	30 ± 3	3.56 ± 0.4	33 ± 3	3.1 ± 0.35	35 ± 2
	2.15%	5.1 ± 0.11	40 ± 3	5 ± 0.19	41 ± 6	4.9 ± 0.31	42 ± 5	4.9 ± 0.19	38 ± 5
28 nm	1.5%	4.2 ± 0.13	35 ± 4	4 ± 0.11	38 ± 3	3.8 ± 0.21	36 ± 2.5	3.5 ± 0.20	28 ± 2
	2.15%	5.0 ± 0.10	50 ± 2.5	5.11 ± 0.15	51 ± 4	5.2 ± 0.13	52 ± 3.5	4.9 ± 0.24	52 ± 5
32 nm	1.5%	5.02 ± 0.2	33 ± 4	5 ± 0.16	31 ± 2	4.6 ± 0.21	32 ± 5	4 ± 0.16	30 ± 4
	2.15%	6.4 ± 0.18	50 ± 2	6.1 ± 0.17	50 ± 6	5.9 ± 0.24	50 ± 6	5 ± 0.21	50 ± 3

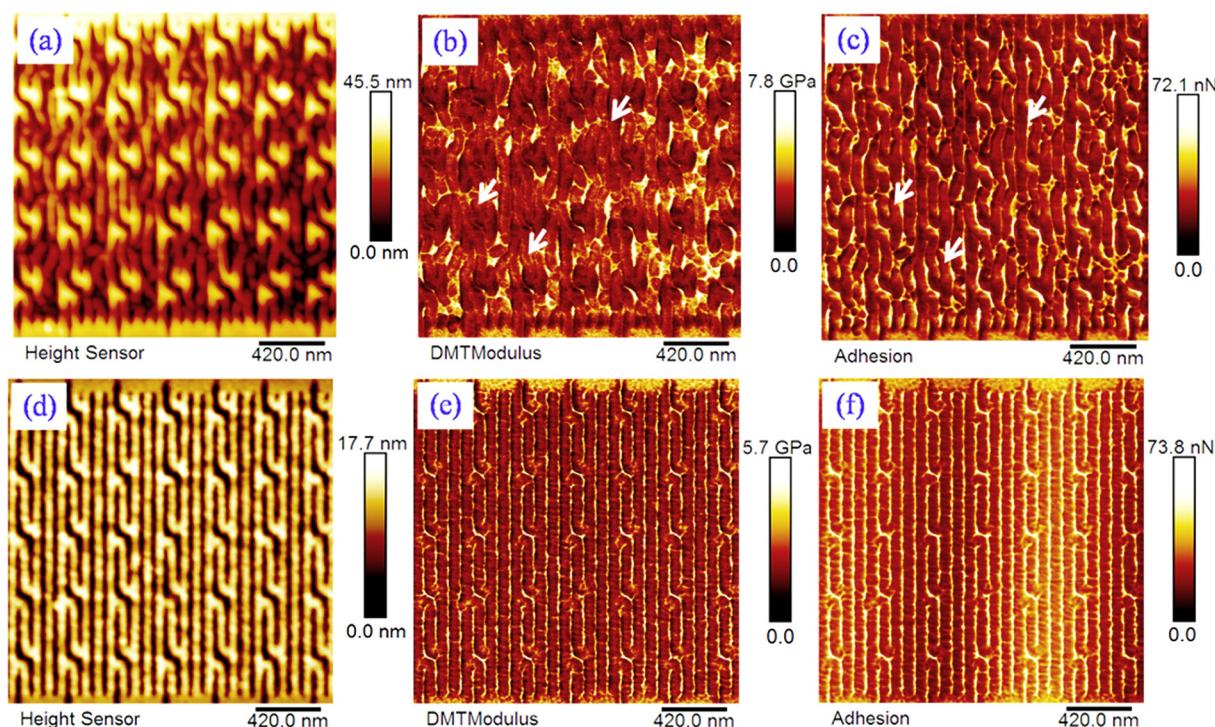


Fig. 8. PF-QNM topography, DMT modulus and tip-sample adhesion force mapping images of 40 nm line-elbow connections structure for (a)–(c) 1.5% resist and (d)–(f) 2.15 resist formulation, respectively.

thickness of the resists features resulting from the line fracturing at higher resolutions. The calculated DMT modulus and tip-sample adhesion force values obtained from line-elbow complex features of 1.5% resist were 3 GPa and 30 nN respectively (see, Fig. 8(b)–(c)). The similar PF-QNM measurements also performed on the complex nanopatterns obtained from 2.15% resist (see, Fig. 8(d)–(f)). The line-elbow connections patterned from the 2.15% resists were shown in Fig. 8d and the corresponding DMT modulus as well as tip-sample adhesion forces map are shown in Fig. 8(e) and (f) respectively. The DMT modulus and tip-sample adhesion values obtained for these features were 4 GPa and 32 nN respectively.

The detailed analyses of the DMT modulus and tip-sample adhesion force obtained from the different complex nano-features (boat, waves and line-elbows) were given in the Supplementary materials (Table S1). In short, the results of these studies also suggest that the complex nanopatterns obtained from 2.15% resist exhibiting better mechanical properties and hence less pattern collapse as compared to those of the 1.5% resist patterns.

As noticed, the increased amounts of SbF_6^- in 2.15% resist resulted in enhanced modulus value (5 GPa) in comparison to the 1.5% resist and other MAPDST based resists reported in the literature such as PMMA [28], MAPDST-*i*-PrMA copolymer (3 GPa) [35] and HfO_2 -methacrylate-MAPDST hybrid resist (3.1 GPa) [23]. A considerable increase in the modulus and adhesion makes the patterns obtained from 2.15% resist stiffer thus reducing the swelling, buckling, peel off and hence the pattern collapse. As already mentioned earlier, the reported procedures to increase the modulus of a resist include the addition of crosslinkers to the resist formulation, which may also lead to adverse effects such as resist swelling during the development processes [24,31–33]. In the present study, an increase in the percentage of the inorganic component SbF_6^- in the resist formulation appears to have helped in improving the modulus and surface properties of the resist, perhaps in an indirect manner.

Finally, all the above studies demonstrate that the 2.15% resist patterns show improved mechanical properties and less pattern collapse compared to those of the 1.5% resist patterns. It is to be noted here that

a number of factors such as the thickness of the resist, composition of the resist formulation, exposure dose, geometry of the patterns etc. may affect the mechanical properties exhibited by a resist pattern. Therefore, in the present study, we had attempted to keep most of these initial parameters constant for the two resists studied except their composition. Therefore, we had spun coated the two resists to the same film thickness, i.e. 45 nm, to have a uniform film thickness, geometry and aspect ratio for their patterns. However, due to compositional differences, the 1.5% and 2.15% resists exhibited different EUV exposure doses, i.e. 96 and 33 mJ/cm^2 respectively. It is known that the variations in exposure dose may affect the pattern geometry, tip-adhesion forces and mechanical properties, especially for negative tone resists. A previous study on the exposure dose-dependent nanoscale modulus analysis on resist patterns revealed that the modulus of the resist increases with increase in the exposure dose [25,43]. Whereas, in the present study, metal content was different in the two resist formulations studied, which led to a lower modulus at higher exposure dose ($\sim 96 \text{ mJ}/\text{cm}^2$) for 1.5% resist and a higher modulus at a lower exposure dose (33 mJ/cm^2) for 2.15% resist, as desired for next-generation EUVL applications. Similarly, in previous reports, the thickness dependence of the resists has been shown, i.e. the modulus increases with the decrease in the film thickness. Our investigation results differ from these reports as the 2.15% resist has a higher final film thickness (25 nm) and high modulus (~ 5 GPa), while the 1.5% resist has lower film thickness (18.5 nm) and lower modulus (3 GPa) [21,44,45]. Hence we may exclude the thickness & EUV dose dependence effect in the present study. The polydispersity of the two polymers were also different (1.59 and 2.67 respectively for the 1.5% and 2.15% resists), which could also have significantly influenced the observed results. Considering all these, it is not easy to identify the exact reasons behind the improved mechanical as well as pattern collapse properties exhibited by the 2.15% resist patterns compared to those of the 1.5% resist patterns. Therefore, more detailed studies are required to identify the exact roles played by each of the contributing parameters such as compositional difference, roles of exposure dose, aspect ratios, etc. in deciding the final outcome of the present study. Details of such analyses

will be presented in a separate study.

4. Conclusions

In summary, we have investigated two hybrid resists, i.e., 1.5%–& 2.15%– MAPDSA-MAPDST copolymers, having different percentages of SbF_6^- content for the nano-mechanical properties of their resist patterns by PF-QNM analyses. These studies revealed that the compositional difference of the two resists leads to further differences in their lithographic properties including differences in EUV exposure dose, geometry and aspect ratios of the EUV patterns etc. It is concluded that the final outcome of all these differences is an overall enhancement in the modulus and tip-sample adhesion force values of the resist patterns obtained from 2.15% resist compared to those of the 1.5% resist. Due to the superior mechanical properties, collapse free line patterns resulted for all the experimented L/S features ranging from L/5S-L/2S in the case of 2.15% resist as compared to 1.5% resist. In short, an increased amount of SbF_6^- content in MAPDSA-MAPDST copolymer resists has shown a positive impact on the modulus and tip-sample adhesion force values calculated for the line patterns as well as complex features obtained from EUVL exposure. More detailed studies are required to understand the roles played by factors like exposure dose, geometry and aspect ratios of the patterns, polydispersity differences etc. in the observed enhancement in the mechanical properties of the patterns in the case of 2.15% resist.

Acknowledgements

Authors acknowledge Intel Corp USA for partial support of the project administered by SRC USA. The use of the Microfield Exposure Tool (MET) at LBNL is also gratefully acknowledged. P.G. Reddy thanks the Council of Scientific and Industrial Research (CSIR), New Delhi, India for a Senior Research Fellowship.

Appendix A. Supplementary data

Supplementary data to this article can be found online at <https://doi.org/10.1016/j.mee.2018.03.014>.

References

- [1] G.E. Moore, Cramming more components onto integrated circuit, *Electronics* 38 (1965) 114–117.
- [2] G. Tallents, E. Wagenaars, G. Pert, Optical lithography: lithography at EUV wavelengths, *Nat. Photonics* 4 (2010) 809–811.
- [3] H.P. Alesso, C.F. Smith, *Connections: Patterns of Discovery*, John Wiley & Sons, New Jersey, 2008.
- [4] S. Ghosh, C.P. Pradeep, S.K. Sharma, P.G. Reddy, S.P. Pal, K.E. Gonsalves, Recent advances in non-chemically amplified photoresists for next generation IC technology, *RSC Adv.* 6 (2016) 74462–74481.
- [5] N. Mojarad, J. Gobrecht, Y. Ekinci, Beyond EUV lithography: a comparative study of efficient photoresists' performance, *Sci. Rep.* 5 (2015) 9235.
- [6] S. Oda, D. Ferry, *Silicon nanoelectronics*, Taylor and Francis, Boca Raton, USA, 2006.
- [7] R.F. Pease, S.Y. Chou, Lithography and other patterning techniques for future electronics, *Proc. IEEE* 96 (2008) 248–270.
- [8] D.P. Sanders, Advances in patterning materials for 193 nm immersion lithography, *Chem. Rev.* 110 (2010) 321–360.
- [9] F. Watt, A.A. Bettiol, J.A. Vankan, E.J. Teo, M.B.H. Breese, On beam lithography and nano-fabrication: a review, *Int. J. Nanosci.* 4 (2005) 269–286.
- [10] N. Mojarad, M. Hojeij, L. Wang, J. Gobrecht, Y. Ekinci, Single-digit-resolution nanopatterning with extreme ultraviolet light for the 2.5 nm technology node and beyond, *Nano* 7 (2015) 4031–4037.
- [11] B. Wu, A. Kumar, Extreme ultraviolet lithography: a review, *J. Vac. Sci. Technol. B* 25 (2007) 1743.
- [12] T. Itani, T. Kozawa, Resist materials and processes for extreme ultraviolet lithography, *Jpn. J. Appl. Phys.* 52 (2013) 010002.
- [13] K.J. Lawrie, I. Blakey, J.P. Blinco, H.H. Cheng, R. Gronheid, K.S. Jack, I. Pollentier, M.J. Leeson, T.R. Younkin, A.K. Whittaker, Chain scission resists for extreme ultraviolet lithography based on high performance polysulfone-containing polymers, *J. Mater. Chem.* 21 (2011) 5629–5637.
- [14] N. Niina, H. Kudo, H. Oizumi, T. Itani, T. Nishikubo, Synthesis and property of noria (water-wheel like macrocycle) derivatives with pendant alkoxy and adamantyl ester groups, and their application for extreme ultraviolet resist, *Thin Solid Films* 534 (2013) 459–464.
- [15] R.D. Re, J. Passarelli, M. Sortland, B. Cardineau, Y. Ekinci, E. Buitrago, M. Neisser, D.A. Freedman, R.L. Brainard, Low-line edge roughness extreme ultraviolet photoresists of organotin carboxylates, *J. Micro. Nanolith. MEMS MOEMS* 14 (2015) 043506.
- [16] M. Sortland, J. Hotalen, R.D. Re, J. Passarelli, M. Murphy, T.S. Kulmala, Y. Ekinci, M. Neisser, D.A. Freedman, R.L. Brainard, Platinum and palladium oxalates: positive-tone extreme ultraviolet resists, *J. Micro./Nanolith. MEMS MOEMS* 14 (2015) 043511.
- [17] W.J. Bae, M. Trikeriotis, J. Sha, E.L. Schwartz, R. Rodriguez, P. Zimmerman, E.P. Giannelis, C.K. Ober, High refractive index and high transparency HfO_2 nanocomposites for next generation lithography, *J. Mater. Chem.* 20 (2010) 5186–5189.
- [18] L. Li, S. Chakrabarty, K. Spyrou, C.K. Ober, E.P. Giannelis, Studying the mechanism of hybrid nanoparticle photoresists: effect of particle size on photopatterning, *Chem. Mater.* 27 (2015) 5027–5031.
- [19] H.H. Solak, Y. Ekinci, P. Käser, S. Park, nm half-pitch resolution Photon-beam lithography reaches 12.5, *J. Vac. Sci. Technol. B* 25 (2007) 91.
- [20] R.A. Lawson, L.M. Tolbert, C.L. Henderson, High sensitivity nonchemically amplified molecular resists based on photosensitive dissolution inhibitors, *Vac. Sci. Technol. B* 28 (2010) C6S12.
- [21] W.M. Yeh, D.E. Noga, R.A. Lawson, L.M. Tolbert, C.L. Henderson, Comparison of positive tone versus negative tone resist pattern collapse behavior, *J. Vac. Sci. Technol. B* 28 (2010) C6S6.
- [22] J.W. Thackeray, Materials challenges for sub-20-nm lithography, *J. Micro./Nanolithogr. MEMS, MOEMS* 10 (2011) 033009.
- [23] P.G. Reddy, N. Mamidi, P. Kumar, S.K. Sharma, S. Ghosh, K.E. Gonsalves, C.P. Pradeep, Design, development, EUVL applications and nano mechanical properties of a new HfO_2 based hybrid non-chemically amplified resist, *RSC Adv.* 6 (2016) 67143–67149.
- [24] T. Tanaka, M. Morigami, N. Atoda, Mechanism of resist pattern collapse during development process, *Jpn. J. Appl. Phys.* 32 (1993) 6059.
- [25] P.K. Kulshreshtha, K. Maruyama, S. Kiani, D. Ziegler, J. Blackwell, D. Olynick, P.D. Ashby, Nanoscale modulus and surface chemistry characterization for collapse free resists, *Proc. SPIE* 8681 (2013) 868100.
- [26] H.B. Cao, P.F. Nealey, W.D. Domke, Comparison of resist collapse properties for deep ultraviolet and 193 nm resist platforms, *J. Vac. Sci. Technol. B* 18 (2000) 3303–3307.
- [27] T.R. Böhme, J.J. de Pablo, Evidence for size-dependent mechanical properties from simulations of nanoscopic polymeric structures, *J. Chem. Phys.* 116 (2002) 9939.
- [28] S.P. Delcambre, R.A. Riggleman, J.J. de Pablo, P.F. Nealey, Mechanical properties of antiplasticized polymer nanostructures, *Soft Mater.* 6 (2010) 2475–2483.
- [29] D.Z. Burton, B. Bhushan, Hydrophobicity, adhesion, and friction properties of nanopatterned polymers and scale dependence for micro- and nanoelectromechanical systems, *Nano Lett.* 5 (2005) 1607–1613.
- [30] H. Nakagawa, T. Naruoka, T. Nagai, Recent EUV resists toward high volume manufacturing, *J. Photopolym. Sci. Technol.* 27 (2014) 739–756.
- [31] T.A. Brunner, C.A. Fonseca, Optimum tone for various feature types: positive versus negative, *Proc. SPIE* 4345 (2001) 30.
- [32] J. Dai, S.W. Chang, A. Hamad, D. Yang, N. Felix, C.K. Ober, Molecular glass resists for high-resolution patterning, *Chem. Mater.* 18 (2006) 3404.
- [33] P.K. Kulshreshtha, K. Maruyama, S. Kiani, J. Blackwell, D.L. Olynick, P.D. Ashby, Harnessing entropic and enthalpic contributions to create a negative tone chemically amplified molecular resist for high-resolution lithography, *Nanotechnology* 25 (2014) 315301.
- [34] G. Winroth, R. Gronheid, T.G. Kim, P.W. Mertens, Strength analysis of EUV-exposed photo resists by AFM at 40 nm half pitch and below, *Microelectron. Eng.* 98 (2012) 159.
- [35] S.K. Sharma, S.P. Pal, P.G. Reddy, P. Kumar, S. Ghosh, K.E. Gonsalves, Design and development of low activation energy based nonchemically amplified resists (n-CARs) for next generation EUV lithography, *Microelectron. Eng.* 164 (2016) 115–122.
- [36] M. Lorenzoni, L. Evangelio, S. Verhaeghe, C. Nicolet, C. Navarro, F. Pérez-Murano, Assessing the local nanomechanical properties of self-assembled block copolymer thin films by peak force tapping, *Langmuir* 31 (2015) 11630–11638.
- [37] O. Krivosheeva, M. Sababi, A. Dedaite, P.M. Claesson, Nanostructured composite layers of mussel adhesive protein and ceria nanoparticles, *Langmuir* 29 (2013) 9551–9561.
- [38] P.G. Reddy, P. Kumar, S. Ghosh, C.P. Pradeep, S.K. Sharma, Kenneth E. Gonsalves, Organic–inorganic hybrid photoresists containing hexafluoroantimonate: design, synthesis and high resolution EUV lithography studies, *Mater. Chem. Front.* 1 (2017) 2613–2619.
- [39] K.E. Gonsalves, S. Ghosh, C.P. Pradeep, G. Reddy, S.K. Sharma, P. Kumar, *Indian Pat. Appl. IN* 2016-11022219, (2016).
- [40] M.E. Dokukin, I. Sokolov, Macromolecules, on the Measurements of Rigidity Modulus of Soft Materials in Nanoindentation Experiments at Small Depth, 45 (2012), pp. 4277–4288.
- [41] S. Ghosh, V.S.V. Satyanarayana, B. Pramanick, S.K. Sharma, C.P. Pradeep, I.M. Reyes, N. Batina, K.E. Gonsalves, Patterning highly ordered arrays of complex nanostructures through EUV directed polarity switching of nonchemically amplified photoresist, *Sci. Rep.* 6 (2016) 22664.
- [42] J.M. Torres, C.M. Stafford, B.D. Vogt, Manipulation of the elastic modulus of polymers at the nanoscale: influence of UV–ozone cross-linking and plasticizer, *ACS Nano* 4 (2010) 5357–5365.
- [43] P. Kulshreshtha, K. Maruyamac, S. Dhuey, D. Ziegler, W. Chao, Paul Ashby,

- D. Olynick, Revealing beam-induced chemistry using modulus mapping in negative-tone EUV/e-beam resists with and without cross-linker additives, *Proc. SPIE* 9425 (2015) 942501.
- [44] R.-C. Chang, F.-Y. Chen, P.-H. Yang, Mechanical properties of photoresist thin films at various temperature, *J. Chin. Soc. Mech. Eng.* 27 (2006) 237–242.
- [45] B.R. Frieberg, K.A. Page, J.R. Graybill, M.L. Walker, C.M. Stafford, G.R. Stafford, C.L. Soles, Mechanical response of thermally annealed nafion thin films, *ACS Appl. Mater. Interfaces* 8 (2016) 33240–33249.